Title
Classical molecular dynamics simulation of electronically non-adiabatic processes

Authors
Miller, William H
Cotton, Stephen J

Publication Date
2016-12-22

DOI
10.1039/c6fd00181e

Peer reviewed

Faraday Discussions

Cite this: *Faraday Discuss.*, 2016, **195**, 9

PAPER

Classical molecular dynamics simulation of electronically non-adiabatic processes

William H. Miller* and Stephen J. Cotton

Received 29th August 2016, Accepted 2nd September 2016
DOI: 10.1039/c6fd00181e

Both classical and quantum mechanics (as well as hybrids thereof, *i.e.*, semiclassical approaches) find widespread use in simulating dynamical processes in molecular systems. For large chemical systems, however, which involve potential energy surfaces (PES) of general/arbitrary form, it is usually the case that only classical molecular dynamics (MD) approaches are feasible, and their use is thus ubiquitous nowadays, at least for chemical processes involving dynamics on a single PES (*i.e.*, within a single Born–Oppenheimer electronic state). This paper reviews recent developments in an approach which extends standard classical MD methods to the treatment of electronically non-adiabatic processes, *i.e.*, those that involve transitions between different electronic states. The approach treats nuclear and electronic degrees of freedom (DOF) equivalently (*i.e.*, by classical mechanics, thereby retaining the simplicity of standard MD), and provides "quantization" of the electronic states through a symmetrical quasi-classical (SQC) windowing model. The approach is seen to be capable of treating extreme regimes of strong and weak coupling between the electronic states, as well as accurately describing coherence effects in the electronic DOF (including the de-coherence of such effects caused by coupling to the nuclear DOF). A survey of recent applications is presented to illustrate the performance of the approach. Also described is a newly developed variation on the original SQC model (found universally superior to the original) and a general extension of the SQC model to obtain the full electronic density matrix (at no additional cost/complexity).

1 Introduction

Reaction rate theory, and the theory of chemical dynamics more generally, provides the foundation for a quantitative description of many important practical problems in the chemical sciences. It is also an intrinsically fascinating subject from the perspective of basic physical theory because it involves quantum and classical mechanics in almost equal measure, one or the other being more useful depending on the problem of interest. Quantum mechanics (QM) is of

Department of Chemistry and Kenneth S. Pitzer Center for Theoretical Chemistry, University of California, and Chemical Sciences Division, Lawrence Berkeley National Laboratory, Berkeley, California 94720, USA. E-mail: MillerWH@berkeley.edu; StephenJCotton47@gmail.com

course always correct (it is the "theory of everything" in molecular science), but accurate calculations with it are limited to molecular systems that are not too large (although this size continues to increase with time) or special forms of the quantum Hamiltonian. Classical mechanics (CM), on the other hand, while only approximate on the molecular scale, can be applied to extremely large systems with essentially arbitrary interaction potentials. Semiclassical (SC) approaches, which use classical-like approximations to quantum mechanics, try to incorporate some of the advantages of each (the correctness of QM with the applicability of CM), and by providing insight into the classical limit of quantum theory it also finds use in developing various analytic approximations. One sees examples of all these approaches in the papers presented for this Discussion.

As a simulation tool, though, SC methodologies are still considerably more difficult to implement than a completely classical treatment, so classical molecular dynamics (MD) remains the most widely used and often the only applicable approach for simulating the dynamics of large molecular systems. For this reason, in the last 2–3 years we have been exploring the question of how far one can go with a more-or-less standard classical MD simulation approach in treating electronically non-adiabatic processes. Electronic non-adiabaticity is, of course, a key feature in many important molecular processes—about 30 percent of the papers in this Discussion deal with electronically non-adiabatic dynamics—so if such an approach can treat a wide class of these processes to an acceptable level of accuracy, it would be a useful addition to theoretical capabilities.

The purpose of this paper is to review such an approach for treating processes involving electronically non-adiabatic dynamics,[1–8] one which involves some very old ideas, but with some more recent updates that have made it remarkably accurate for a variety of applications that have been carried out to date. Rather than a "mixed quantum–classical" approach (*i.e.*, electrons treated quantum mechanically and nuclei classically), it treats the dynamics of all degrees of freedom (DOF), nuclear and electronic, by classical mechanics, thus providing a dynamically consistent (albeit classical) description of their interaction.

The two key ingredients that make up the overall approach are (i) how electronic DOF are described by classical mechanics, and (ii) how electronic state information is recovered from a classical MD simulation. The first step uses the Meyer–Miller[9] (MM) classical representation for electronic DOF (summarized in Section 2) together with the standard classical description of the nuclear DOF, and the second uses a symmetrical quasi-classical (SQC) model[1,2] to "quantize" the electronic DOF initially and finally (described in Section 3). The overall approach will thus be referred to as SQC/MM, and its most attractive feature (apart from how well it works) is its simplicity and straight-forward implementation *via* standard classical MD simulation protocols. A review of some of its recent applications is given in Section 4, and further/future model development is discussed in Section 5.

It is worthwhile noting that the MM vibronic (*i.e.*, nuclear + electronic) Hamiltonian—which can be derived in various ways, heuristic or more rigorous[10]—is actually an exact Hamiltonian in the sense that if the classical nuclear and electronic coordinates and momenta variables were all replaced by quantum mechanical operators in the standard way, and the resulting Hamiltonian operator used in the Schrödinger equation, this would provide an exact description of the quantum vibronic dynamics. Thus, the approximation is that

both nuclear and electronic DOF are treated classically, *i.e.*, by computing classical trajectories in these nuclear and electronic variables.

The symmetrical quasi-classical (SQC) model for extracting electronic state information from such classical trajectories (in order, *e.g.*, to calculate transition probabilities from one electronic state to another) evolved from the quasi-classical (QC) trajectory method for obtaining ro-vibrational state information from classical trajectory calculations (on a single potential energy surface); this is a natural way to proceed since the electronic DOF in the MM representation are harmonic oscillators. Key to its success has been some useful "tweaks" that have been added to the original QC technique in the intervening years: the "symmetrical" idea suggested[11] many years ago but not pursued, Stock's suggestion[12,13] of including less than the full zero point energy (ZPE) in the "electronic oscillators" of the MM model, and Bonnet *et al.*'s[14] introduction of window functions of reduced size (though not applied symmetrically). We also emphasize in the presentation of Section 3 that the SQC model can be thought of as the "classical Wigner model" (which emerges from various semiclassical approaches), provided that the Wigner functions are defined appropriately.

2 Classical representation of the electronic degrees of freedom

The Meyer–Miller (MM) model provides a classical description of the electronic degrees of freedom for a finite set (F, say) of electronic states. It has been described and reviewed many times, so only its salient features will be discussed here. In its original presentation, the MM model[9] characterizes each electronic state k by a pair of classical harmonic oscillator action-angle variables (n_k, q_k), and if ($\mathbf{P}$, $\mathbf{R}$) are the nuclear momenta and coordinates, the MM classical Hamiltonian for the nuclear and electronic DOF is

$$H(\mathbf{P},\mathbf{R},\mathbf{n},\mathbf{q}) = \frac{|\mathbf{P}|^2}{2\mu} + \sum_k^F n_k H_{k,k}(\mathbf{R}) + 2\sum_{k<k'}^F \sqrt{n_k+\gamma}\sqrt{n_{k'}+\gamma}\cos\left(q_k - q_{k'}\right) H_{k,k'}(\mathbf{R}), \quad (1)$$

where the $F \times F$ diabatic electronic matrix $\{H_{k,k'}(\mathbf{R})\}$ (assumed here to be real symmetric) depends parametrically on the nuclear coordinates and in principle comes from many-electron quantum chemistry. (Of practical importance, there is an equivalent adiabatic version derived in Appendix B of the original MM paper.[9]) The electronic and nuclear dynamics are determined by computing classical trajectories from this Hamiltonian (by integrating Hamilton's equations) for electronic and nuclear DOF. This was the primary goal of the MM approach: to have a consistent dynamical description of electronic and nuclear DOF that treated both in an equivalent framework.

In MM's heuristic derivation of eqn (1), the parameter γ was inserted into the off-diagonal coupling elements and taken to be $\frac{1}{2}$ on the basis of semiclassical considerations (*e.g.*, since Bohr–Sommerfeld quantization gives half-integer values of the classical action). This effectively provided each electronic DOF with a half-integer quantum of ZPE, beneficially causing there to be a dependence of

final action variables $\{n_k\}$ on the initial angles $\{q_k\}$. Stock[12,13] later found in some of his applications that better results were obtained by choosing $\gamma < \frac{1}{2}$ (suggesting a "best value" of $\approx\frac{1}{4}$) so as to incorporate only a fraction of the full ZPE. We have also generally viewed γ as an empirical parameter (chosen between 0 and $\frac{1}{2}$), though the value $\frac{\sqrt{3}-1}{2}\approx 0.366$ has some theoretical justification,[2] and a very similar value of $\gamma = \frac{1}{3}$ arises naturally in our new SQC windowing model (discussed below) from purely geometric considerations;[7] either of these values is essentially optimal depending on the windowing model employed.

In nearly all applications of the MM model, Hamilton's equations have not been integrated directly in action-angle variables $\{n_k, q_k\}$ themselves, but rather in the Cartesian variables $\{p_k, x_k\}$ that are related to them *via* the following canonical transformation,

$$p_k = -\sqrt{2(n_k+\gamma)}\,\sin(q_k) \tag{2a}$$

$$x_k = \sqrt{2(n_k+\gamma)}\,\cos(q_k), \tag{2b}$$

in terms of which the Hamiltonian of eqn (1) becomes

$$H(\mathbf{P},\mathbf{R},\mathbf{p},\mathbf{x}) = \frac{|\mathbf{P}|^2}{2\mu} + \sum_k^F \left(\frac{1}{2}{p_k}^2 + \frac{1}{2}{x_k}^2 - \gamma\right) H_{k,k}(\mathbf{R}) + \sum_{k<k'}^F \left(p_k p_{k'} + x_k x_{k'}\right) H_{k,k'}(\mathbf{R}). \tag{3}$$

The procedure is thus to specify initial conditions in terms of action-angle variables (see below), change to the initial conditions for the Cartesian variables *via* eqn (2), integrate Hamilton's equations (for nuclear and electronic variables) as generated from the Hamiltonian of eqn (3), and then, at the final time, compute the final action variables $\{n_k\}$ *via* the inverse of eqn (2):

$$n_k = \frac{1}{2}{p_k}^2 + \frac{1}{2}{x_k}^2 - \gamma. \tag{4}$$

The MM representation thus characterizes the F electronic states as F (coupled) harmonic oscillators, the excitation of which represents the occupation of that electronic state, and electronic transitions emerge in this picture as "vibrational" transitions between these "electronic oscillators". Electronic state k thus corresponds to the direct product of F harmonic oscillator states, all of which are in their ground state (no quanta) except the kth mode which has one quantum of excitation,

$$|k\rangle = \underbrace{|0,\cdots,n_k=1,\cdots,0\rangle}_{F\text{-states}}. \tag{5}$$

Because a classical simulation with the MM Hamiltonian adds only F vibrational-like DOF (for the electronic states) to the set of (perhaps very many) nuclear DOF, it is thus typically a very modest addition to a MD simulation for the nuclear DOF alone—provided, of course, that one has the potential energy surfaces (PES) for the various electronic states and their couplings (either through rigorous "quantum chemistry" (*e.g.*, computed "on-the-fly"), less-rigorous density

functional theory (DFT), or possibly from a semi-empirical "molecular mechanics" force field as often used in bio-molecular simulations).

Finally, it should also be noted that although the classical dynamics resulting from the MM Hamiltonian was noted from its origin to be "Ehrenfest dynamics"—*i.e.*, the force on the nuclei at any time is the coherent average over all electronic states—we have explained how the boundary conditions implicit in the SQC procedure (see below) eliminate the Ehrenfest method's well-known deficiency of emerging from a region of electronic coupling in an intermediate electronic configuration; *i.e.*, the equations of motion generated from the MM Hamiltonian are Ehrenfest, but the SQC boundary conditions are not; relatedly, we have shown how the SQC boundary conditions insure that detailed balance is described in a reasonable way[4] (though not necessarily exactly).

3 Symmetrical windowing of the electronic states

The symmetrical quasi-classical (SQC) windowing procedure has been presented previously as arising from an averaging (or smoothing) of the Bohr–Sommerfeld (semiclassical) quantization of the initial and final electronic action variables.[11] Here we give a somewhat different presentation, starting with the exact quantum expressions before invoking the classical limit.

A general *A*–*B* quantum time correlation function has the form

$$C_{AB}(t) = \mathrm{tr}[\hat{A}\, \mathrm{e}^{\mathrm{i}\hat{H}t/\hbar}\hat{B}\, \mathrm{e}^{-\mathrm{i}\hat{H}t/\hbar}] \equiv \mathrm{tr}[\hat{A}\hat{B}(t)], \tag{6}$$

where the operators $\hat{A}$, $\hat{B}$, and the Hamiltonian $\hat{H}$ all operate in the full dimension of all DOF (here electronic and nuclear), and $\hat{B}(t)$ is the Heisenberg time-evolved operator. For the case

$$\hat{A} = \hat{\rho}_{\mathrm{nu}}|i\rangle\langle i|, \quad \hat{B} = |f\rangle\langle f|, \tag{7}$$

where i and f are the initial and final electronic states (the nuclear part of $\hat{B}$ is the identity) and $\hat{\rho}_{\mathrm{nu}}$ is the initial density operator for the nuclear DOF (often the Boltzmann operator for the initial electronic state, but not necessarily so), eqn (6) is the time-dependent electronic transition probability,

$$C_{AB}(t) \rightarrow P_{f\leftarrow i}(t) \equiv \langle |f\rangle\langle f| \rangle_t, \tag{8}$$

where the average is over the initial density operator ($\hat{A}$) of the nuclear and electronic DOF. More generally, if $\hat{B}$ is the off-diagonal density (matrix) operator,

$$\hat{B} = |j\rangle\langle k|, \tag{9}$$

eqn (6) is the time-dependent electronic (*i.e.*, "reduced") density matrix

$$C_{AB}(t) \rightarrow P_{j,k}(t) \equiv \langle |j\rangle\langle k| \rangle_t. \tag{10}$$

The classical Wigner approximation[15–20] (which comes about from several semiclassical approaches, *e.g.*, by linearizing the difference between the forward and backward time evolution operators[21] in the Heisenberg time evolution of eqn

(6)) gives the traditional classical limit, whereby the trace in eqn (6) becomes a phase space average over the initial conditions of classical trajectories (for all DOF), $\hat{A}$ becomes the Wigner function at the initial point in phase space, and $\hat{B}$ the Wigner function at the (classically) time-evolved phase point. For $\hat{A}$ and $\hat{B}$ of eqn (7), the classical transition probability for the $i \rightarrow f$ electronic transition is thus given by

$$C_{AB}(t) \xrightarrow[\text{Classical}]{} \frac{1}{(2\pi\hbar)^{F+G}} \int \mathbf{dP\ dR\ dn\ dq}\ W_{\text{nu}}(\mathbf{P},\mathbf{R}) \cdot W_i(\mathbf{n},\mathbf{q}) \cdot W_f(\mathbf{n_t},\mathbf{q_t}), \qquad (11)$$

where action-angle variables of the "electronic oscillators" are used since the initial and final electronic states are defined in terms of them. The Wigner function W_{nu} for the initial nuclear DOF is the traditional Wigner function of nuclear coordinates and momenta (**R**, **P**), and those for the electronic density (matrix) operators are obtained from the direct product (*cf.* eqn (5)) of 1D harmonic oscillator states for the "electronic oscillators". In the past, these latter Wigner functions were obtained by first calculating them in the Cartesian oscillator variables $\{p_k, x_k\}$ and then transforming to action-angle variables by eqn (2), but it has recently been pointed out[7] that one obtains different Wigner functions which are more consistent with semiclassical theory by carrying out the Wigner integral transform directly in action-angle variables. For a diagonal element of the density operator this gives (for F electronic states)

$$W_k(\mathbf{n},\mathbf{q}) = \delta(n_k - 1) \prod_{l \neq k}^{F} \delta(n_l), \qquad (12)$$

i.e., the electronic oscillators for electronic state k have one quantum of excitation in the kth oscillator, with all others being in the ground vibrational state; it is independent of the angle variables, and recognized to be a statement of Bohr–Sommerfeld quantization (*i.e.*, integer values of the action variables and a random distribution of the angle variables). For the off-diagonal elements of the electronic density operator, one obtains

$$W_{jk}(\mathbf{n},\mathbf{q}) = \mathrm{e}^{-\mathrm{i}(q_j - q_k)} \cdot \delta\left(n_j - \frac{1}{2}\right) \cdot \delta\left(n_k - \frac{1}{2}\right) \prod_{l \neq j,k}^{F} \delta(n_l), \qquad (13)$$

which can be shown to be equivalent to the Heisenberg Correspondence Principle (a semiclassical approximation for off-diagonal matrix elements); since these depend on the angle variables (which are the classical phase of the harmonic oscillators) they carry electronic phase information.

In both eqn (12) and (13), the SQC approach is to replace the delta functions by "pre-limit" delta functions—or "window" functions—localized about the integer (or half integer) action variables. This not only makes the calculations much simpler, but the smoothing effect this entails brings the classical results into much better agreement with quantum results *versus* using the delta functions themselves.[22] There is, of course, no unique pre-limit delta function, and this is where the modelistic aspect of the SQC model enters; one uses intuition and experience to choose these "window" functions to be as universally capable of treating as wide a range of situations as possible.

In practice, therefore, one samples initial conditions (by Monte Carlo) from the initial phase space distribution in eqn (11), initial electronic actions being

sampled from the selected window function (with conjugate angles chosen randomly between 0 and 2π), and after integrating Hamilton's equations (generated from the MM Hamiltonian) for electronic and nuclear DOF to any desired time t, "collecting" the final electronic actions in the window functions corresponding to all final electronic states of interest (also applying window functions for off-diagonal elements of the electronic density matrix, and accumulating the electronic phase factor as dictated by eqn (13), if these elements are of additional interest).

4 Test applications

Presented here is a sample of applications that have recently been carried out using the SQC/MM approach for a variety of non-adiabatic benchmark problems. While it is unlikely that such a simple, purely-classical methodology can provide quantitative accuracy in all cases—*e.g.*, where true tunnelling in the nuclear DOF is necessary to reach a region of non-adiabatic coupling—the following examples illustrate some of the breadth that the approach has been able to achieve.

We begin with examples in the regime of moderate to very strong non-adiabatic coupling between the electronic states, first for simple 1D scattering (where there is at least one avoided crossing between two PES), and then for a more realistic model of non-adiabatic dynamics in condensed phases (*via* standard spin–boson and related site–exciton models).

Considered next is the limit of weak electronically non-adiabatic coupling, a regime where we have expected the original SQC/MM model to fail (for understandable reasons). By analyzing the weak-coupling limit, a new SQC windowing methodology has been developed[8] which not only deals with the anticipated problem of weak-coupling, but is also seen to perform even better than our original model in essentially all coupling regimes. It is also interesting that the value of the ZPE γ-parameter (see eqn (1) and related discussion) is set in this new windowing scheme based on purely geometric considerations (though the value is still consistent with our prior analytical justifications and empirical observations).

We conclude with application to two site–exciton models: (i) a 7-site model of the Fenna–Matthews–Olson (FMO) complex in order to illustrate the treatment of a problem (with the original SQC/MM approach) involving a higher number of electronic states, and (ii) a simpler 2-state site–exciton model which illustrates the use of eqn (13) to calculate the full electronic density matrix.

4.1 Moderate to strong (to very strong) coupling between the electronic states

4.1.1 1D Scattering: single and dual avoided crossings (Tully 1 and 2). In devising his fewest switches surface hopping (FSSH) model, Tully[23] used several simple 1D 2-state scattering problems that have become popular benchmarks; the Tully 1 and Tully 2 problems illustrate treatment of single or dual avoided crossings of two PES. The results of applying the SQC/MM approach to these problems are presented in Fig. 1, and good agreement is observed. There is electronic coherence structure exhibited in the dual avoided crossing problem (Tully 2) which is accurately captured in the SQC/MM calculations. This may at first seem surprising—*i.e.*, that quantum coherence effects are well described by

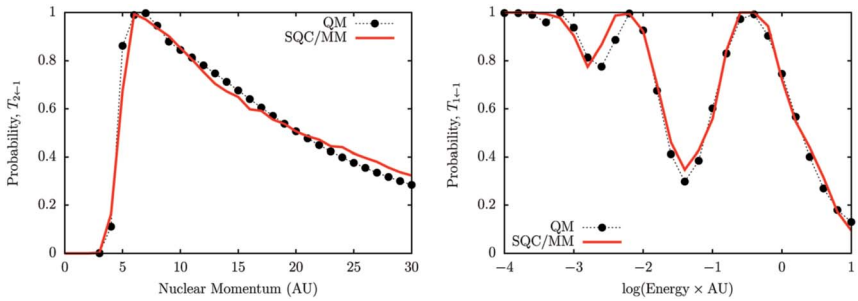

Fig. 1 Tully 1 and 2 problems: single avoided crossing (left) and dual avoided crossing (right).

a fully classical MD calculation—but it is a consequence of the fact that the classical dynamics of the electronic oscillators generated by the MM Hamiltonian, eqn (3), is equivalent to the time-dependent electronic Schrödinger equation (for a given nuclear trajectory); *i.e.*, quantum coherence in the electronic DOF is encoded in the classical coherence of the electronic oscillators by this classical vibronic Hamiltonian.

4.1.2 Spin–boson problems. Electronically non-adiabatic processes in a condensed phase environment are often modeled with the well-known spin–boson (SB) problem, which corresponds to taking the diagonal elements of the diabatic electronic matrix to be harmonic oscillators (displaced in position and energy); the off-diagonal elements are usually taken to be constants. This "harmonic bath" of nuclear DOF dissipates/absorbs electronic energy and leads to decoherence in the electronic DOF. The model is commonly given by:

$$\mathbf{H}(\mathbf{Q}) = \begin{bmatrix} V_0(\mathbf{Q}) + V_1(\mathbf{Q}) + \varepsilon & \Delta \\ \Delta & V_0(\mathbf{Q}) - V_1(\mathbf{Q}) - \varepsilon \end{bmatrix}, \tag{14}$$

where

$$V_0(\mathbf{Q}) = \sum_{k=1}^{G} \frac{1}{2}\omega_k{}^2 Q_k{}^2 \quad \text{and} \quad V_1(\mathbf{Q}) = \sum_{k=1}^{G} c_k Q_k,$$

2ε being the energetic bias and Δ the non-adiabatic coupling (a constant independent of nuclear coordinates).

The harmonic bath embodied in eqn (14) may be described by a spectral density (SD) function which represents a distribution of vibrational frequencies $\{\omega_k\}$ chosen so as to correspond to a particular condensed phase environment. For simplicity, the SD is often taken to have a continuous functional form which cuts off at high-frequency, and for the benchmark problems considered here, the common exponentially-damped ohmic form is used which is given by

$$J(\omega) = \frac{\pi}{2}\alpha\omega\, \mathrm{e}^{-\omega/\omega_c}, \tag{15}$$

where ω_c is the SD's characteristic frequency and α is the bath coupling (or friction) parameter. Alternatively, a Debye SD is also often used, which is given by

$$J(\omega) = 2\lambda\frac{\omega\omega_c}{\omega^2 + \omega_c{}^2}, \tag{16}$$

where the overall coupling strength is parameterized by the reorganization energy λ (instead of α). In either case, from the relationship

$$J(\omega) = \frac{\pi}{2}\sum_{k=1}^{G}\frac{{c_k}^2}{w_k}\delta(\omega-\omega_k), \tag{17}$$

the coupling strengths $\{c_k\}$ of the local vibrational modes are given by

$$c_k = \sqrt{\frac{2}{\pi}\Delta\omega\omega_k J(\omega_k)} \tag{18}$$

for use in eqn (14).

The standard Wigner distribution function is usually used for the initial conditions of the nuclear/bath DOF,

$$\rho(\mathbf{P},\mathbf{Q}) \propto \prod_{k=1}^{G} \mathrm{e}^{-a_k\cdot\left[\frac{1}{2}{P_k}^2+\frac{1}{2}{\omega_k}^2\left(Q_k+\frac{c_k}{{w_k}^2}\right)^2\right]}, \tag{19}$$

where $a_k = \frac{2}{\omega_k}\tanh\left(\frac{\beta\omega_k}{2}\right)$, which serves to set the effective temperature $T = (k_B\beta)^{-1}$ of the simulation. Note that $G = 100$ bath modes (see eqn (14) and (19)) are used in the calculations below—so of an order relevant to an electronic transition in the condensed phase.

The most interesting aspect of the SB problem is the time-dependent population of the various electronic states and the extent to which coherence effects in them survive or are de-cohered (and how rapidly) by coupling to the nuclear/bath DOF, and the dependence of all this on the "bath" temperature. It is further recognized that the asymmetric variant of the problem—*i.e.*, having energetic bias between the electronic states ($\varepsilon \neq 0$)—is typically much more challenging for simple (and inexpensive) classical methodologies to describe accurately.

Four cases are thus considered in Fig. 2: symmetric and asymmetric versions of the SB problem at high and low temperatures (the same as in ref. 2, 4 and 8, with the parameters as given in the figure caption). Plotted for the four cases *versus* benchmark QM results[24,25] are the SQC/MM-calculated time-dependent population differences between electronic states 1 and 2 ($P_{1\leftarrow 1}(t) - P_{2\leftarrow 1}(t)$) after the system is initialized in electronic state 1. As with the simple Tully 2 problem, it is seen that the SQC/MM methodology is able to do a good job of quantitatively capturing the electronic coherence (and decoherence) in the exact results for all four parameter regimes, as well as correctly describing the long-time limit. It should be emphasized that no special "de-coherence effects" (*i.e.*, corrections) need be added to the theory; the coherence structure comes about (or not) and decoheres naturally (if present) from the interaction of the nuclear and electronic DOF as generated by the classical mechanics of the MM Hamiltonian (and is extracted from the dynamics by the windowing methodology).

4.1.3 Very strong electronic coupling: Bellonzi *et al.*'s spin–boson problem. A version of the SB problem was recently used by Bellonzi *et al.*[26] to provide a strenuous test of the accuracy of various simple non-adiabatic approaches in the regime of very strong electronic coupling. The model is essentially equivalent to eqn (14) with the distribution of harmonic modes given by the Debye SD of eqn (16) (instead of the ohmic form of eqn (15) used in the examples of Fig. 2) and with

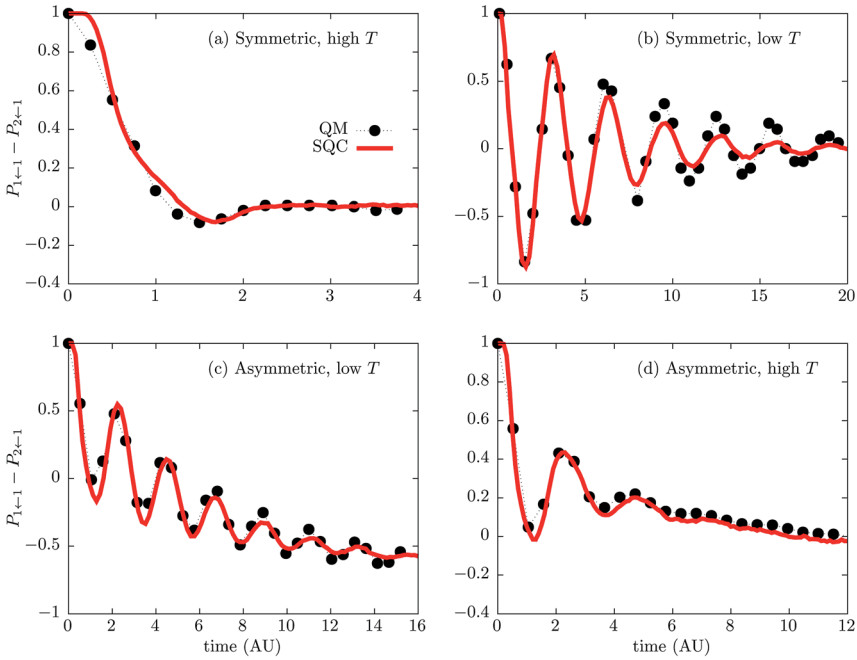

Fig. 2 Symmetric ($\varepsilon = 0$) and asymmetric ($\varepsilon = 1$) spin–boson benchmark problems at high and low temperature treated with SQC/MM approach *versus* exact QM results;[24,25] parameters corresponding to eqn (14), (15), and (19): case (a) $\alpha = 0.09$, $\beta\Delta = 0.1$, $\omega_c = 2.5\Delta$; case (b) $\alpha = 0.09$, $\beta\Delta = 5$, $\omega_c = 2.5\Delta$; case (c) $\alpha = 0.1$, $\beta\Delta = 5$, $\omega_c = 2.5\Delta$; case (d) $\alpha = 0.1$, $\beta\Delta = 0.25$, $\omega_c = \Delta$.

the electronic coupling constant Δ assigned various multiples of $k_B T$ (with these and other parameters as given in the figure caption).

Fig. 3 consists of six panels showing Bellonzi *et al.*'s results† for the population decay of initial state 1, $P_{1\leftarrow1}(t)$, calculated using the standard fewest-switches surface hopping (FSSH) procedure and the mean-field/Ehrenfest (MF) method, plotted against their benchmark HEOM results. The different panels correspond to three values of electronic coupling strength of $\Delta = \{1, 2, 3\} \times k_B T$ (top to bottom in Fig. 3), at short and long (10×) times (left to right). Overlaid on these results for each of the six panels are our SQC/MM results, computed in the same manner as the other SQC/MM results reported here except that $G = 500$ modes were used to discretize the bath DOF (as opposed to $G = 100$ for the SB calculations in Fig. 2).

† N. Bellonzi and J. E. Subotnik, private communication of results for the strong coupling model in ref. 26. It was noted that due to difficulty in converging the FSSH (fewest-switches surface hopping) and MF (Ehrenfest) calculations with a Debye SD (*i.e.*, eqn (16), as would correspond to the HEOM result), the FSSH and MF calculations instead employed the SD of eqn (28) of ref. 26; we understand that these FSSH results are in better agreement with the benchmark HEOM calculations (because they were better converged) despite using a different SD. (Also, we note that the result corresponding to the middle coupling strength ($2 \times k_B T$) in Fig. 3 looks very similar (if not identical) to the corresponding FSSH result shown in Fig. 7 of ref. 26, which was calculated using a Debye SD, reinforcing the suggestion that the different SD's give essentially the same results in this case.)

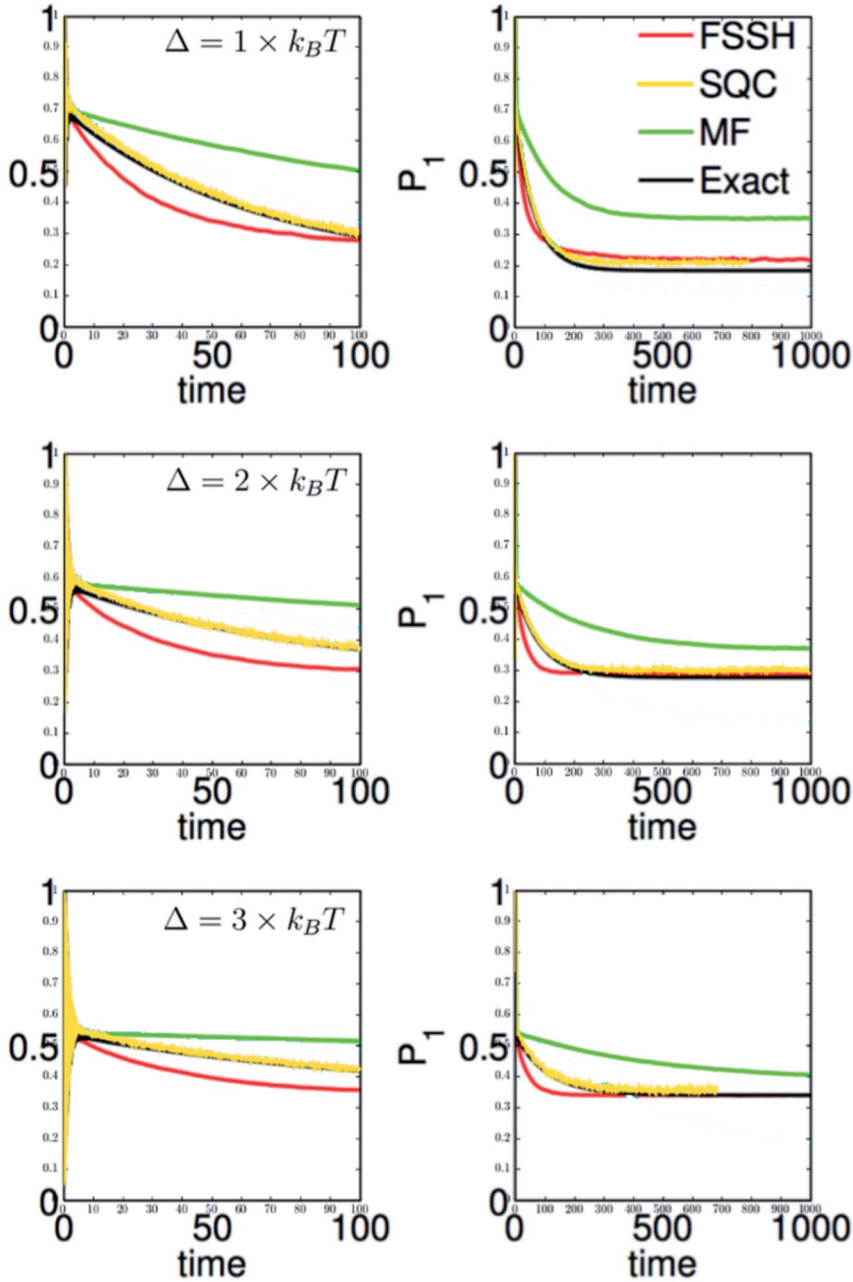

Fig. 3 Bellonzi *et al.*'s asymmetric ($\varepsilon = 5$) SB problem[26] with very strong electronic coupling ($\Delta = \{1, 2, 3\} \times k_B T$ where $k_B T$ is taken to be 5 (in AU)); the Debye SD of eqn (16) was used with $\lambda = 1.25$ and $\omega_c = 0.25$ (in AU); displayed are Bellonzi *et al.*'s benchmark HEOM results (black curves), FSSH results (red curves), and MF/Ehrenfest results (green curves), along with our SQC/MM results (yellow curves).

Several conclusions are evident from the data in Fig. 3: first, with regard to the long-time limit of the population decay (right panels), for each of the three coupling strengths, the figure shows that both the FSSH and SQC/MM approaches reproduce the correct long-time limits, matching what is obtained from the benchmark HEOM calculations, while the conventional Ehrenfest (MF) method does not.

For the shorter time scales (as magnified in the left panels of Fig. 3), however, it is clear that only the SQC/MM approach reproduces the short-time dynamics quantitatively (as determined by the benchmark HEOM results). Looking closely at Fig. 3 one sees that the oscillations in the decay curves are so rapid at short time—$t \lesssim 5$ in the plots (left)—that they appear coalesced as a vertical block (of yellow for SQC/MM, and beneath it, black for HEOM), a consequence of the extremely strong electronic coupling in these examples (relative to the other parameters) in comparison to the oscillation/coupling time-scales of the SB problems shown in Fig. 2. These results are thus quite significant in the sheer strength of the electronic coupling presented in this application, and the results thus provide an interesting and well-defined comparison between the MF, FSSH and SQC/MM methodologies in this extreme limit.

In summary, the SQC/MM methodology is seen to perform quite well in the regimes of moderate to strong to very strong coupling between the electronic states. Ironically, it is the weak-coupling regime (discussed next) which poses a severe problem for the SQC/MM approach in its original implementation.

4.2 Weak coupling

4.2.1 Analysis and SQC model development. It is easy to understand why the standard SQC model used so far fails to treat the weak-coupling limit properly: the origin of the problem lies in the definition of the windowing functions. Up to this point, we have exclusively relied on simple square histogram windowing functions as the pre-limit delta-functions to be used in eqn (11) and (12) (*i.e.*, "boxes" of width 2γ centered at the quantum integer values of the electronic action variables). Fig. 4 illustrates such square histogram window functions for the case of $F = 2$ electronic states, and shows that for our preferred value of $\gamma = 0.366$ there is a gap between the windows defining the two states.

For moderately and strongly coupled problems (*e.g.*, having transition probabilities $\gtrsim 0.1$), the presence of this gap between the windows poses no issue. However, as we have recently discussed,[8] for weak coupling between the electronic states, the action variables (n_1, n_2) originating in the windowing function defining one state in Fig. 4 will move only slightly during the course of a simulation—they would not move at all if the coupling were zero—and thus (because of the gap) none of them will reach the window function defining the other state, yielding (after renormalization) a zero transition probability. This deficiency can be remedied by having the window functions touch at a point in the action space so that even for very small coupling a small number of trajectories will reach the window function defining the other state, but for the square histogram windows shown in Fig. 4 this would entail setting $\gamma = \frac{1}{2}$ which we know from experience generates much poorer results for problems having "normal" transition probabilities ($\gtrsim 0.1$), thus leading to the undesirable possibility of having to use a value for γ that depends on the strength of the electronic coupling.

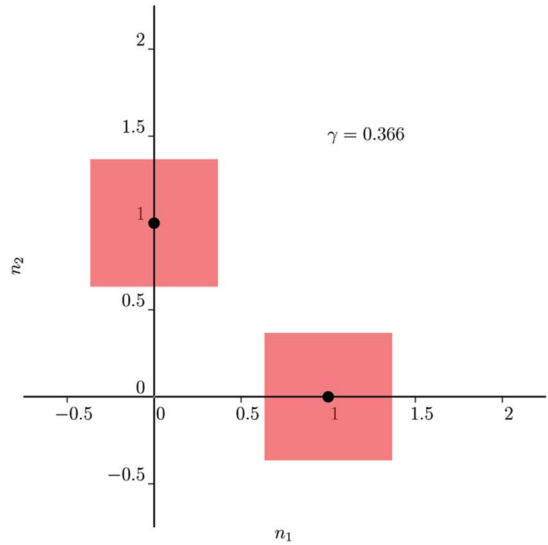

Fig. 4 Square histogram windows, with $\gamma = 0.366$, for the electronic action variables of two electronic states; black dots show the integer quantum values of the actions for the two states.

A surprising solution to this dilemma is a new SQC windowing model[8] based on triangle-shaped window functions. These functions do touch at a point in the electronic action space, but they retain a value of γ in the neighborhood of what we know from experience to be optimal. The new SQC triangle windowing scheme is shown in Fig. 5 for the value of $\gamma = \frac{1}{3}$ along with the previous square histogram model (of the same γ). In the square histogram model, γ sets the width of the window functions. In the triangle scheme, γ instead adjusts the position of the windows in the action space (their size is fixed so that they touch). The value of $\gamma = \frac{1}{3}$ is the unique value which places the centroids (center points) of these unit-length isosceles right triangles at the quantum values of the action variables ($(n_1, n_2) = (1, 0)$ for state 1, and $(n_1, n_2) = (0, 1)$ for state 2) as shown in Fig. 5. Thus, unlike the square histogram scheme where γ was viewed as an empirical parameter setting the size of the histogram windows and whose optimal value was arrived at through numerical "experimentation" (and separately justified on independent theoretical grounds[2]), for these triangle windows, the "right" value of γ (*i.e.*, $\frac{1}{3}$) is uniquely determined from purely geometric considerations.

4.2.2 Tully 1 revisited. Though this new SQC model with triangle window functions was devised in order to properly treat the limit of very weak electronic coupling (and it does so quite well), it has also been found to perform even better in the "normal" coupling regime than our previous standard model (with square histogram windows);[8] *i.e.*, the new scheme performs *universally* better than the prior standard model in all coupling regimes, while being no more complicated to implement (and also likely to be superior from the standpoint of numerical convergence). Recent work[8] presents applications to a variety of model problems that validate the new methodology; here we briefly show results for a weakly-coupled version of the Tully 1 problem, as the simplest non-trivial example

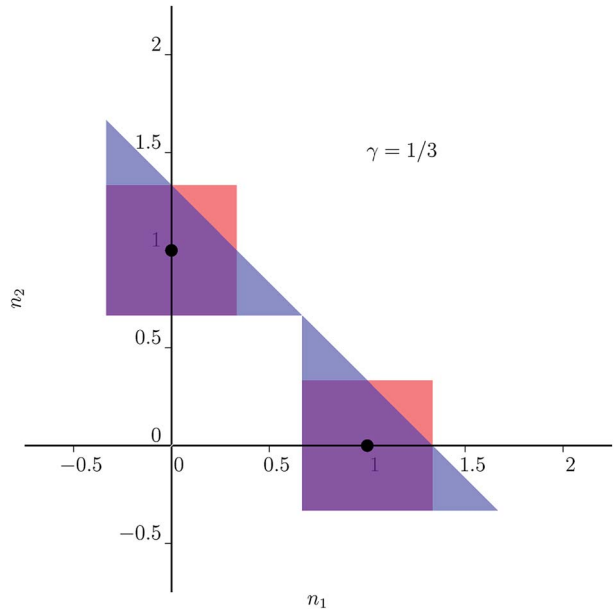

Fig. 5 Triangle (blue) and square histogram (red) window functions (with dots indicating quantum centers).

illustrating the failure of the previous histogram windowing scheme in the weak-coupling limit and the excellent treatment provided by the new SQC triangle methodology.

In its original form Tully 1 is a very strongly coupled problem (as shown in Fig. 1), but it may be turned into a weakly coupled problem by reducing the strength of the off-diagonal element of the diabatic Hamiltonian matrix (which is real symmetric),

$$H_{12}(R) = C\,\mathrm{e}^{-R^2}, \tag{20}$$

i.e., by reducing the value of the parameter C.

Fig. 6 shows (on a log–log scale) the SQC-calculated $T_{2\leftarrow 1}$ transmission probabilities for Tully 1 using both the triangle and square histogram window functions computed over a broad range of values for the parameter C—from its original value of 0.005 down to 10^{-5}—for a fixed value of the initial nuclear momentum ($P = 15$ AU, in the middle of the momentum range for Tully 1 shown in Fig. 1).‡ Also shown are the exact QM benchmark results, and the anticipated failure of the original SQC square histogram methodology in the weak coupling limit is readily apparent: deviations from the correct non-adiabatic transition probability begin to appear for transition probabilities around 10%, with very

‡ Rigorous energy-domain QM scattering calculations for the Tully 1 problem reveal "Feshbach resonances" around the peak in transmission shown in Fig. 1 which are not present in time-domain wave-packet scattering calculations and which become more pronounced as the non-adiabatic coupling is reduced. To focus on the weak-coupling issue, the selected value of nuclear momenta is away from these resonances.

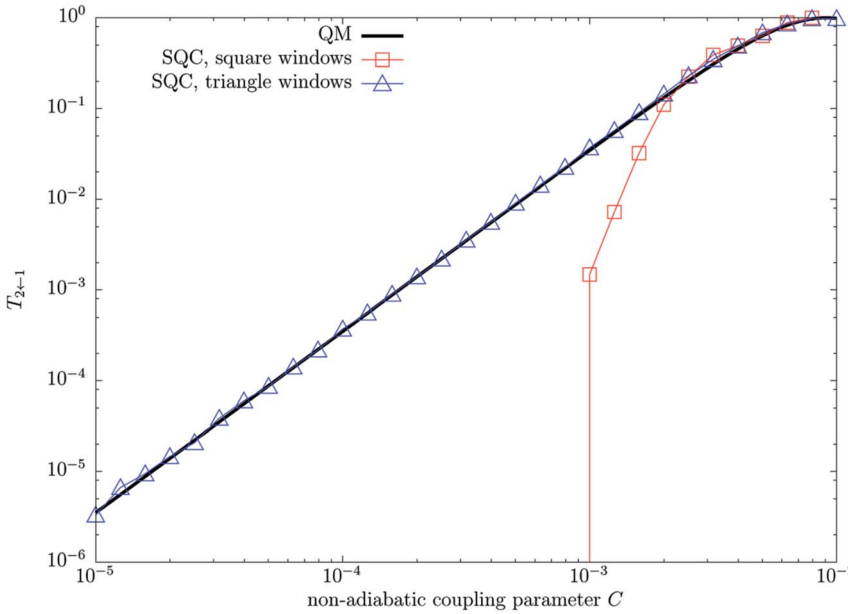

Fig. 6 SQC/MM results calculated using square histogram and triangle window functions *versus* energy-domain QM scattering calculations ($P = 15$ AU).

significant deviations for transition probabilities around 1%; below that, the SQC transition probability is essentially zero.

It is thus striking to see how effective the new windowing scheme is in describing the weak coupling regime with no additional effort or cost: simply by re-shaping the original SQC square histogram pre-limit delta functions into triangles, one is able to capture the correct QM transmission probabilities down to 10^{-5} with quantitative accuracy (and without disturbing the prior good results obtained with the SQC methodology in the "normal" coupling regime). Further results[8] indicate that these conclusions (regarding the new windowing) generalize to the treatment of more complicated non-adiabatic systems, for example to treating the site–exciton Hamiltonian (below) used to model an electronic excitation hopping from site-to-site in a condensed phase having hundreds of nuclear DOF interacting with the electronic dynamics.

4.3 Application to more than 2 states: the 7 site FMO complex

Though most models of non-adiabatic processes treat only two electronic states, the SQC/MM methodology can also be applied to systems with any number of electronic states, and the oft-studied 7-state site–exciton model of the Fenna–Matthews–Olson (FMO) complex provides a convenient benchmark example to illustrate this.[6]

For two states, the site–exciton (SE) Hamiltonian[28] is very similar to the SB Hamiltonian given above in eqn (14), the primary difference being that in the SE model the two electronic states correspond to whether one or the other of two "sites" is electronically excited, and also that each such site is coupled to its own

independent harmonic bath (the notion being that the nuclear DOF about each site may be different). The electronic Hamiltonian matrix for two sites is thus given by:

$$\mathbf{H}(\mathbf{Q}) = \begin{bmatrix} V_{\mathrm{bath}}^{(1)}(\mathbf{Q}-\mathbf{D}) + V_{\mathrm{bath}}^{(2)}(\mathbf{Q}) + \varepsilon_1 & \Delta_{12} \\ \Delta_{12} & V_{\mathrm{bath}}^{(1)}(\mathbf{Q}) + V_{\mathrm{bath}}^{(2)}(\mathbf{Q}-\mathbf{D}) + \varepsilon_2 \end{bmatrix}, \quad (21)$$

where $\{\varepsilon_k\}$ are the site energies, Δ_{12} is the non-adiabatic coupling constant between sites/states 1 and 2, and

$$V_{\mathrm{bath}}^{(k)}(\mathbf{Q}) = \sum_{\xi \in \substack{\text{site } k \\ \text{modes}}}^{G} \frac{1}{2}\omega_\xi^{\,2} Q_\xi^{\,2}. \quad (22)$$

For the general case of F sites/states, there is an $F \times F$ matrix of site energies $\{\varepsilon_k\}$ and coupling constants $\{\Delta_{k,k'}\}$, with the kth diagonal element of the electronic Hamiltonian matrix given by

$$H_{k,k}(\mathbf{Q}) = V_{\mathrm{bath}}^{(k)}(\mathbf{Q}-\mathbf{D}) + \sum_{k' \neq k}^{F} V_{\mathrm{bath}}^{(k')}(\mathbf{Q}) + \varepsilon_k, \quad (23)$$

again showing the kth state being an electronic configuration with a single excitation at the kth site. For the benchmark problems considered here, the bath vibrational modes $\{\omega_\xi\}$ of eqn (22) are characterized by the Debye SD of eqn (16) (parameterized by the reorganization energy λ) with the coupling constants $\mathbf{D} \equiv \{D_\xi\}$ in eqn (21) and (23) given by

$$D_\xi = \sqrt{\frac{2}{\pi}\frac{\Delta\omega}{\omega_\xi^{\,3}} J(\omega_\xi)}. \quad (24)$$

All the SQC/MM calculations shown here employed $G = 200$ bath modes per site in eqn (22). Thus, for 2 sites, the calculations used $2 \times G = 400$ nuclear DOF plus $F = 2$ electronic DOF, and for the 7-site FMO model, $7 \times G = 1400$ nuclear DOF plus $F = 7$ electronic DOF.

While there are newer model Hamiltonians for the FMO complex advocated in the literature, Ishizaki & Fleming's original (7-site/state) version[27]—along with their essentially exact (HEOM) calculations—serves as a well-defined benchmark for evaluating the performance of the SQC/MM methodology. SQC/MM calculations for this system are shown in Fig. 7 and 8 along with the benchmark HEOM results (with the parameters as given in the figure captions).

The results in Fig. 7 correspond to the FMO complex having the initial electronic excitation at site 1, and the SQC/MM calculations are seen to agree reasonably well with the HEOM results, *e.g.*, the overall participation of the various states in causing the decay of population from state 1, the coherence/decoherence patterns, *etc.*, are described well. The most noticeable deviation of the SQC/MM calculation from the correct HEOM result is that the long time decay of state 1 (predominantly to state 3) is about 20% faster than that given by the HEOM calculation.

Fig. 8 shows analogous calculations for the initial excitation being on site/pigment 6. In this case the time-evolution of the electronic coherence structure and the overall multi-state dynamics is considerably more complex than what is seen in Fig. 7, with all 7 states showing some coherence structure in the first 200

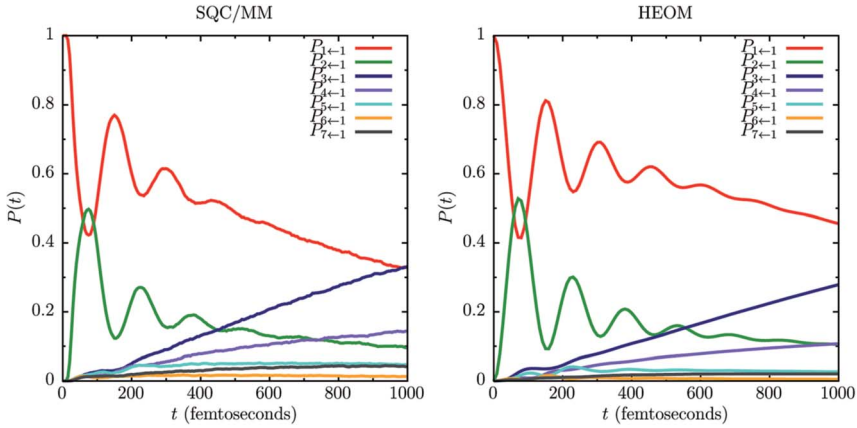

Fig. 7 SQC/MM and benchmark HEOM results for 7-state FMO model; $T = 77$ K, $\lambda = 35$ cm^{-1}, $\omega_c = 106.14$ cm^{-1}; the matrix of site energies $\{\varepsilon_k\}$ and non-adiabatic couplings $\{\Delta_{k,k'}\}$ are given in ref. 27 (see Fig. 2a of ref. 27).

femtoseconds, and 5 of the 7 states receiving significant electronic excitation by the end of the 1 picosecond simulation. Here the SQC calculation does an excellent job of replicating the exact HEOM result, exhibiting no substantial deviations from it.

Fig. 7 and 8 thus demonstrate application of the SQC/MM approach to larger numbers of electronic states, showing a good description of condensed-phase "quantum" coherence/de-coherence effects, just as was seen (above) for the 2-state examples.

4.4 Example calculation of the full electronic density matrix

As discussed in Section 3, the SQC windowing methodology may be viewed formally as an approximate implementation of Bohr–Sommerfeld quantization

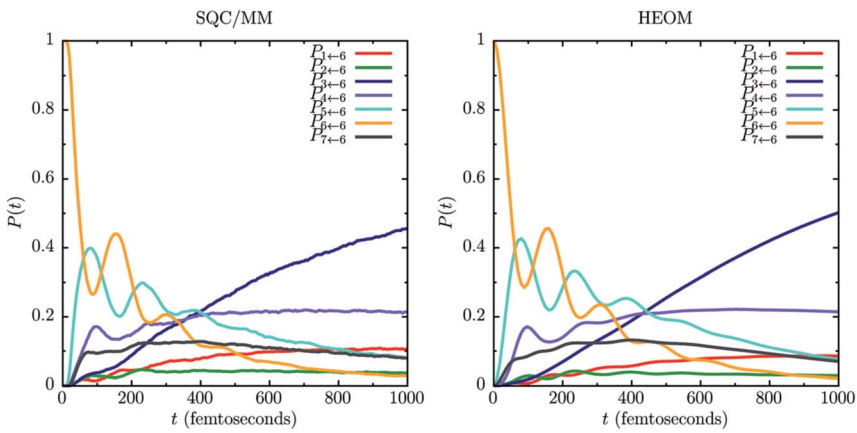

Fig. 8 SQC/MM and HEOM results for 7-state FMO model; same as Fig. 7 except site 6 (instead of site 1) is initialized as electronically excited (see Fig. 2b of ref. 27).

through the use of Wigner functions calculated directly in terms of action-angle variables. A practical consequence of this view is that it provides a simple prescription for using window functions (*i.e.*, pre-limit delta functions in eqn (13)) to extract the off-diagonal elements of the electronic density matrix (*i.e.*, the "quantum" coherences between the electronic states) from the same classical trajectory simulation used to obtain the diagonal elements (the electronic state populations), and to do so at essentially little or no additional cost.

To proceed with such a calculation, it is natural to choose the windowing scheme shown in Fig. 9 which defines the window function for the off-diagonal element of the density matrix, ρ_{12}, to be a square histogram "box" (red window) centered at $(\frac{1}{2}, \frac{1}{2})$ having the same width 2γ as the window functions for the electronic state populations (blue windows) centered at (1, 0) and (0, 1). Calculation of $\rho_{12}(t)$ then simply entails monitoring trajectories as they evolve in the electronic action-space (n_1, n_2) and for those which happen to be within the ρ_{12} (red) window function at time t, calculating their average phase factor $e^{-i(q_1(t)-q_2(t))}$. (Note that the phase-factor also makes the window function for ρ_{12} orthogonal to the other windows despite their overlap in the action-space as shown in Fig. 9.)

An example calculation of the full time-dependent electronic density matrix is shown in Fig. 10 for a 2-state version of the SE model given above in eqn (21) (with the parameters as given in the figure caption). One sees that this simple procedure provides a very good description of the time-dependence of the real and imaginary parts of the ρ_{12} density matrix element, in addition to yielding excellent results for the electronic populations (ρ_{11} and ρ_{22}).

4.5 Other issues

The development of this SQC treatment of the MM classical vibronic model is clearly an ongoing process, and as one finds new areas where it has problems one

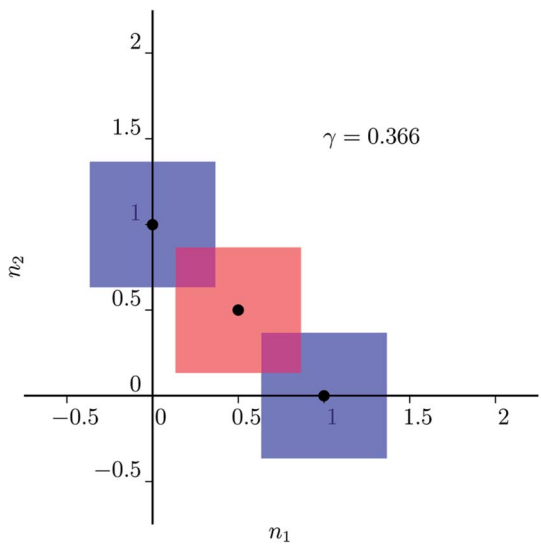

Fig. 9 SQC window functions for the diagonal (blue) and off-diagonal (red) elements of the density matrix applied to a system of 2 electronic states.

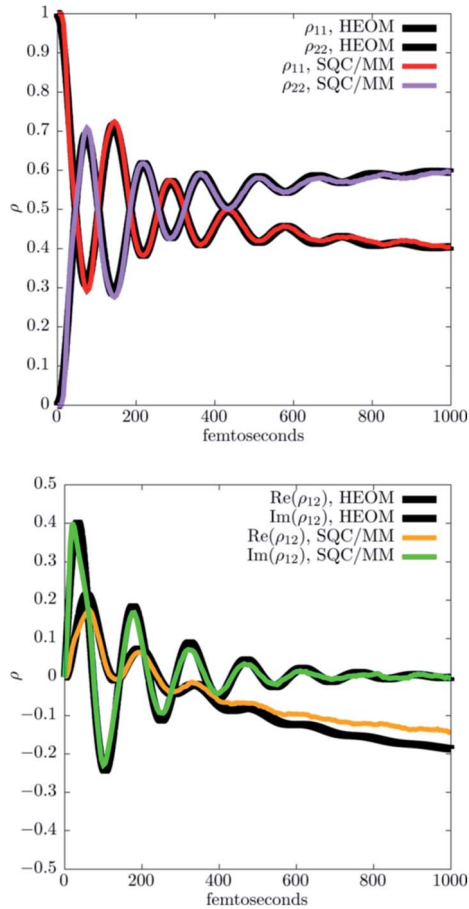

Fig. 10 SQC/MM computed density matrix $\{\rho_{ij}(t)\}$ *versus* HEOM results for 2-state site–exciton model (difference in site energies $\varepsilon_1 - \varepsilon_2 = 100$ cm^{-1}, non-adiabatic coupling $\Delta = 100$ cm^{-1}, bath characteristic frequency $\omega_c = 53.08$ cm^{-1}, reorganization energy $\lambda = 20$ cm^{-1}, and $T = 300$ K; see Fig. 4 of ref. 28).

seeks useful remedies that can still be implemented within a standard classical MD protocol. It has been emphasized that the window functions of the SQC model should be thought of as pre-limit delta functions that impose Bohr–Sommerfeld quantization of the initial and final electronic action variables approximately, and since there is no unique pre-limit delta function, this offers the possibility of creative choices to deal with various "issues" as they are discovered. The triangle window functions described in Section 4.2 are an excellent example of this, where it was realized that the standard square histogram window functions would fail in the limit of weak electronic coupling; the triangle windows were designed to deal with this, and they were then found to perform better more generally, for all coupling regimes.

Another problem that has been discussed recently[26] for the SQC/MM approach arises when some of the potential surfaces (*e.g.*, diagonal elements of the diabatic electronic matrix) have very harshly repulsive regions. One can see from eqn (1)

that the action variables for some trajectories can have negative values (their lower limit is $-\gamma$), which will lead to potentials that are thus extremely attractive and cause the nuclear trajectory to diverge ("run away"). This problem was seen earlier[29] when classical trajectories from the MM Hamiltonian were used as input to the "initial value representation" of semiclassical theory (SC-IVR). In these earlier applications it was seen that some trajectories diverged, but since they were typically no more than 10% or so in the Monte Carlo sampling over initial conditions, they were simply discarded and thus caused no significant problem. For the model system treated in ref. 26, however, the vast majority of trajectories diverge, so something else must be done. One very simple approach that we have explored is simply to cut off the strongly repulsive potentials at an energy far above an energy that any classical trajectory would experience; *i.e.*, the repulsive potential is replaced by V_{cut} whenever it is larger than this cutoff value. Testing this idea for the model in ref. 26 yields trajectories none of which diverge, so this particular "issue" is thus really not a problem. Further consideration of such examples, however, is certainly warranted and there may be other even better ways to deal with this.

There will certainly be other situations for which even our most recent versions of the SQC approach will fail, and the challenge will be to see if other simple and useful modifications can be found. What does seem clear to us, however, is that the basic dynamics generated by the MM classical vibronic Hamiltonian is the "correct" dynamics, and the challenge is to extract the relevant quantities from it.

5 Future work

SQC triangle windowing in higher dimensions

Fig. 5 illustrates the SQC triangle and square histogram windowing schemes for the case of 2 electronic states. For the square histogram windows, generalization to higher numbers of states is straightforward and the treatment of the 7-state FMO complex in Fig. 7 and 8 provides an illustration of its effectiveness. It is not immediately clear, however, how the triangle windowing scheme shown in Fig. 5 is properly generalized to more than 2 states. Thus, an area of future work is to consider a generalized version of the SQC triangle model, and to validate it over as many illustrative benchmark problems involving higher numbers of electronic states as possible.

In Fig. 11, as an initial step, we have taken a first version of our higher-dimensional SQC triangle scheme and applied it to a 3-state spin–boson (SB) problem treated by exact QM path-integral methods by Sim & Makri.[30] The SB model is basically a 3-state generalization of that given in eqn (14), and again with the bath DOF described by the ohmic SD of eqn (15). From Fig. 11, it is seen that the agreement between the SQC triangle calculation and the QM result is excellent, and moreover (and perhaps more significantly), only 1000 trajectories were used in this calculation (though 100 nuclear DOF were simulated for the bath). We thus conclude (preliminarily) based on this first proof-of-concept calculation, that a higher-dimensional generalization of the triangle windowing scheme is possible and that it is likely to be quite accurate and efficient (similar to what was discovered to be the case for two electronic states). Subsequent work will provide detailed analysis and model development, as well as further validating calculations.

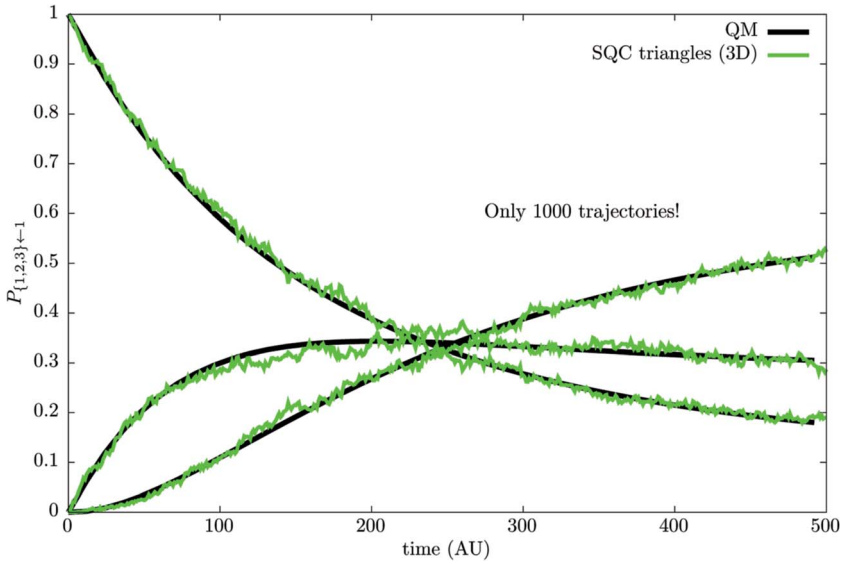

Fig. 11 3-State spin–boson problem of Sim & Makri treated with 3-D triangle SQC windows.

Acknowledgements

We thank Professor David Manolopoulos for his source code to perform the energy-domain quantum scattering calculations for the Tully 1 problem shown in Fig. 6, and Professor Joe Subotnik for providing a pre-print of ref. 26 and useful discussions concerning the strong coupling problem treated in Fig. 3. We also thank Professor Nancy Makri for providing the exact path integral result for the 3-state example shown in Fig. 11. This work was supported by the National Science Foundation under Grant No. CHE-1148645 and by the Director, Office of Science, Office of Basic Energy Sciences, Chemical Sciences, Geosciences, and Biosciences Division, U.S. Department of Energy under Contract No. DE-AC02-05CH11231. In addition, this research utilized computation resources provided by the National Energy Research Scientific Computing Center (NERSC), which is supported by the Office of Science of the U.S. Department of Energy under Contract No. DE-AC02-05CH11231.

References

1 S. J. Cotton and W. H. Miller, *J. Phys. Chem. A*, 2013, **117**, 7190–7194.
2 S. J. Cotton and W. H. Miller, *J. Chem. Phys.*, 2013, **139**, 234112.
3 S. J. Cotton, K. Igumenshchev and W. H. Miller, *J. Chem. Phys.*, 2014, **141**, 084104.
4 W. H. Miller and S. J. Cotton, *J. Chem. Phys.*, 2015, **142**, 131103.
5 S. J. Cotton and W. H. Miller, *J. Phys. Chem. A*, 2015, **119**, 12138–12145.
6 S. J. Cotton and W. H. Miller, *J. Chem. Theory Comput.*, 2016, **12**, 983–991.
7 W. H. Miller and S. J. Cotton, *J. Chem. Phys.*, 2016, **145**, 081102.

8 S. J. Cotton and W. H. Miller, *J. Chem. Phys.*, 2016, **145**, 144108.
9 H.-D. Meyer and W. H. Miller, *J. Chem. Phys.*, 1979, **70**, 3214–3223.
10 G. Stock and M. Thoss, *Phys. Rev. Lett.*, 1997, **78**, 578–581.
11 W. H. Miller and A. W. Raczkowski, *Faraday Discuss. Chem. Soc.*, 1973, **55**, 45–50.
12 G. Stock, *J. Chem. Phys.*, 1995, **103**, 10015–10029.
13 G. Stock, *J. Chem. Phys.*, 1995, **103**, 2888–2902.
14 L. Bonnet and J. C. Rayez, *Chem. Phys. Lett.*, 1997, **277**, 183–190.
15 E. Wigner, *Phys. Rev.*, 1932, **40**, 749–759.
16 W. H. Miller, *J. Chem. Phys.*, 1974, **61**, 1823–1834.
17 W. H. Miller, *J. Chem. Phys.*, 1975, **62**, 1899–1906.
18 S. Chapman, B. C. Garrett and W. H. Miller, *J. Chem. Phys.*, 1975, **63**, 2710–2716.
19 E. J. Heller, *J. Chem. Phys.*, 1976, **65**, 1289–1298.
20 R. C. Brown and E. J. Heller, *J. Chem. Phys.*, 1981, **75**, 186–188.
21 H. Wang, X. Sun and W. H. Miller, *J. Chem. Phys.*, 1998, **108**, 9726–9736.
22 W. H. Miller, *J. Chem. Phys.*, 1971, **54**, 5386–5397.
23 J. C. Tully, *J. Chem. Phys.*, 1990, **93**, 1061–1071.
24 D. E. Makarov and N. Makri, *Chem. Phys. Lett.*, 1994, **221**, 482–491.
25 H. Wang, M. Thoss and W. H. Miller, *J. Chem. Phys.*, 2001, **115**, 2979–2990.
26 N. Bellonzi, A. Jain and J. E. Subotnik, *J. Chem. Phys.*, 2016, **144**, 154110.
27 A. Ishizaki and G. R. Fleming, *Proc. Natl. Acad. Sci. U. S. A.*, 2009, **106**, 17255–17260.
28 A. Ishizaki and G. R. Fleming, *J. Chem. Phys.*, 2009, **130**, 234111.
29 E. A. Coronado, J. Xing and W. H. Miller, *Chem. Phys. Lett.*, 2001, **349**, 521–529.
30 E. Sim and N. Makri, *Comput. Phys. Commun.*, 1997, **99**, 335–354.

